Solvent-Assisted Lipid Bilayer Formation on Au Surfaces: Effect of Lipid Concentration on Solid-Supported Membrane Formation

ORIGINAL PAPER

physica status solidi pss a
www.pss-a.com

Solvent-Assisted Lipid Bilayer Formation on Au Surfaces: Effect of Lipid Concentration on Solid-Supported Membrane Formation

Shova Neupane, Kai Betlem, Frank Uwe Renner, and Patricia Losada-Pérez**

Solvent-assisted lipid bilayer (SALB) formation is emerged as a versatile approach in forming supported lipid membranes (SLBs) on metal surfaces, interesting platforms for transducing a biological signal to an electrical readout where vesicle rupture is not straightforward. Herein, the effect of the lipid concentration in the organic solvent, a key parameter controlling SALB, is addressed in the low and high concentration limits of 1,2-dipalmitoyl-sn-glycero-3-phosphocholine lipid on a Au surface. Quartz crystal microbalance with dissipation (QCM-D) responses are correlated with atomic force microscopy (AFM) topographic and nanomechanical measurements. Upon SALB completion at both concentrations, QCM-D and AFM topographical characterization suggest the formation of thin, although incomplete, lipid layers at the Au–liquid interface, with frequency and dissipation plateau values departing from well-established homogeneous SLB responses. Nanomechanical analysis reveals the presence of mostly monolayers at low concentration due to lack of lipid material, while at high concentration excess of lipid material leads to the coexistence of diverse structures. Their formation stems from the SALB formation mechanism, based on lyotropic transformations upon solvent exchange, which differs from customarily vesicle rupture. Such mechanism leads to peculiar two-step features in approach force curves on SLBs pointing toward a decoupling in bilayer leaflets when supported.

1. Introduction

The complexity of biological membranes makes biomimetic structures a useful approach to study membrane biophysical properties. Among the available biomimetic lipid structures, supported lipid bilayers (SLBs) are very popular 2D platforms to study intrinsic lipid physicochemical properties and their interactions with other molecules such as peptides or drugs.[1–4] Several methods can be used to obtain SLBs on solid surfaces, i.e., Langmuir–Blodgett/Schäfer (LB/S) deposition,[5] lipid vesicle fusion and rupture (VF),[6] spin-coating,[7] and physical vapor deposition.[8] LBS and VF are by far the most used methods to fabricate SLBs. The former yields homogeneous defect-free SLBs, but its use is time-consuming and requires an optimal combination of deposition parameters such as surface pressure and temperature. VF is very straightforward and it relies on vesicle adsorption, deformation, and rupture, which depends strongly on vesicle-surface interactions, thus limiting its applicability to highly hydrophilic surfaces such as mica, SiO_2, and glass. The formation of homogeneous SLBs by VF onto less hydrophilic surfaces such as Au or TiO_2 is more challenging, and it is influenced by the fact that, typically, the adhesion energy between the lipid vesicles and Au is not sufficient to exceed the membrane tension for vesicle rupture.[9–11] VF leads to very heterogeneous layers where local membrane patches are formed combined with intact unruptured vesicles.[12] Importantly, the SLB formation depends strongly on the solid surface topography. As shown by Lipowsky and co-workers, SLB formation is limited on polycrystalline surfaces, while it can take place on large Au grains with atomically flat (111) terraces.[13] The interest in Au resides in its ability to transduce chemical to electrical signals making SLB-coated Au surfaces interesting platforms for electrochemical biosensors and neural electrodes.[14]

An alternative method based on solvent exchange has probed as a versatile approach for forming SLBs on diverse material substrates such as SiO_2,[15–22] Au[17,21,23] nanoporous Au,[24] and Al_2O_3.[17,21] SALB circumvents in principle the drawbacks of VF and enables fabricating SLBs on substrates that do not possess strong enough adhesion energetics for promoting the rupture of vesicles.[11,14] When dissolved in an organic solvent, the lipid molecules are either dissolved as monomers or form inverse micelles.[25] As the organic solvent content progressively decreases, the lipid molecules undergo a series of lyotropic phase transitions

Dr. S. Neupane,[+] Prof. F. U. Renner
Instituut voor Materiaalonderzoek (IMO)
Universiteit Hasselt
Diepenbeek BE-3590, Belgium
E-mail: shova.neupane@chimieparistech.psl.eu

Dr. K. Betlem, Prof. P. Losada-Pérez
Experimental Soft Matter and Thermal Physics (EST) group
Department of Physics
Université Libre de Bruxelles, Boulevard du Triomphe CP223
Brussels 1050, Belgium
E-mail: plosadap@ulb.ac.be

The ORCID identification number(s) for the author(s) of this article can be found under https://doi.org/10.1002/pssa.202000662.

[+]Present address: Division of Physical Chemistry of Surfaces, Institut de Recherche de Chimie Paris Chimie ParisTech-CNRS, 11 rue Pierre et Marie Curie, Paris 75005, France

DOI: 10.1002/pssa.202000662

(monomers, micelles, vesicles). Upon a complete solvent exchange, a SLB is formed at the solid–liquid interface. The SALB protocol is straightforward; it requires minor sample preparation and basic microfluidics. Effective SLB formation needs as well an optimized balance of the lipid concentration and flow rate, as carefully reviewed by Cho and co-workers, establishing an optimal concentration range of SALB formation (0.1–0.5 mg mL^{-1}).[21] The SALB methodology is customarily used using robust techniques like quartz crystal microbalance with dissipation (QCM-D) and fluorescence recovery after photobleaching (FRAP), both providing a global, averaged response of the formation of SLB. Local nanomechanical AFM measurements have indeed confirmed the successful formation of SLBs on glass using 0.5 mg mL^{-1}.[26]

In this work, the effect of lipid concentration (in the organic solvent) on the formation of SLBs on Au surfaces is investigated. QCM-D is combined with FS-AFM to link the averaged global response of solid-supported layer formation to local properties of the layers formed at two different concentrations.

2. Results and Discussion

2.1. Lipid Layer Formation by QCM-D

To form lipid layers on Au surfaces, the protocol introduced by Cho and co-workers was used.[21] First, a baseline is established in HEPES buffer during 15 min. Afterward, HEPES buffer is exchanged with pure isopropanol until a complete solvent exchange is achieved and a new stable baseline is attained. Then, 1,2-dipalmitoyl-sn-glycero-3-phosphocholine (DPPC) dissolved in isopropanol is injected for 15 min, followed by HEPES buffer replacement for 15 min. All the injections are conducted at a small flow rate of 50 µL min^{-1}, ensuring a sufficient contact time between the lipid solution and the surface.[19] **Figure 1** shows a sketch of the SALB experiments using QCM-D, while **Figure 2** shows the overview of QCM-D results, namely, a blank, reference experiment without lipids, SALB with 0.2 and 0.7 mg mL^{-1} DPPC. Each step of the process is labeled with a number: 1) stands for HEPES buffer exchange by isopropanol addition, 2) addition of DPPC dissolved in isopropanol (in the case of the blank measurement only isopropanol was added), and 3) isopropanol exchange by HEPES buffer addition. A sketch of the different steps is depicted in the lowest panel of Figure 1. The solvent exchange leads to large changes in frequency and dissipation responses, Δf_n and ΔD_n, as a result of changes in density and viscosity of the fluids involved. During the mixing of pure fluids, transient behavior (peaks in Δf_n and ΔD_n) is typically observed. Upon a complete solvent exchange, the baselines in Δf and ΔD signals are recovered reaching stable plateau values. DPPC dissolved in isopropanol at different concentrations is then injected in step 2 and a very small decrease in Δf_n ($\Delta f_n < -5$ Hz) and an increase in ΔD_3 ($\Delta D_n < 0.2 \times 10^6$) are observed, indicating the formation of (monolayer or inverted micelle) lipid patches on the Au-coated/buffer interface. The second addition of isopropanol during the reference experiment does not change the plateau values of frequency and dissipation. During step 3 HEPES buffer was injected and a baseline recovered after transient changes in the signals. Final plateau values for Δf and ΔD signals are included in **Table 1**. The formation of a homogeneous and rigid SLB in the fluid phase is characterized by frequency-independent values of Δf_n and ΔD_n, namely, $\Delta f_n \approx -24$ to -27 Hz and $\Delta D_n \leq 0.5 \times 10^{-6}$. In both cases, the plateau values depart slightly from those characterizing the optimal formation of a SLB,[21] indicating the formation of inhomogeneous layers (incomplete bilayer formation, multilayer, trapped vesicles). It should be noted that measurements are conducted at 25 °C, where the lipid bilayers adsorbed on the Au surface are in the gel phase. In this phase, the molecular packing area per lipid (47.5 Å) is smaller than in the fluid phase (70 Å) and thus the surface mass density (and thus Δf_n) in the gel-phase lipid bilayer is larger than in the fluid phase.[27]

2.2. AFM Imaging

After forming the supported lipid layers in the QCM-D flow cells, the Au-coated QCM-D sensors were transferred to the AFM liquid cell to establish a correlation between the QCM-D and AFM measurements. The QCM-D sensors were kept submerged in buffer at all times to guarantee the lipid layers were always hydrated. AFM imaging was performed to characterize the surface topography, and force spectroscopy (FS-AFM) was used to investigate the lipid layers nanomechanical properties. A freshly cleaned gold-coated AFM probe was used to scan the AFM image in contact mode as well as to record the force–distance (F–D) curves.

Figure 3a shows a contact mode AFM image with its corresponding surface roughness histogram of a bare Au electrode in HEPES buffer. It shows a clear polycrystalline texture with grains of lateral size ≈80 nm. Its average surface roughness is $R_a = 1.1 \pm 0.7$ nm. Figure 3b shows a representative image of the layers formed by SALB using 0.2 mg mL^{-1} DPPC on the Au electrode in HEPES buffer. The texture of the surface appears significantly different, the grain boundaries being less sharp and the average surface roughness decreased to $R_a = 0.7 \pm 0.4$ nm.

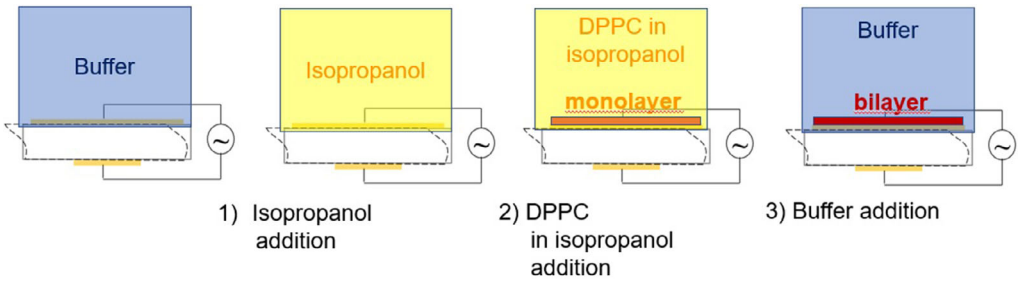

Figure 1. Sketch of the experiments conducted inside a QCM-D flow cell during solvent exchange.

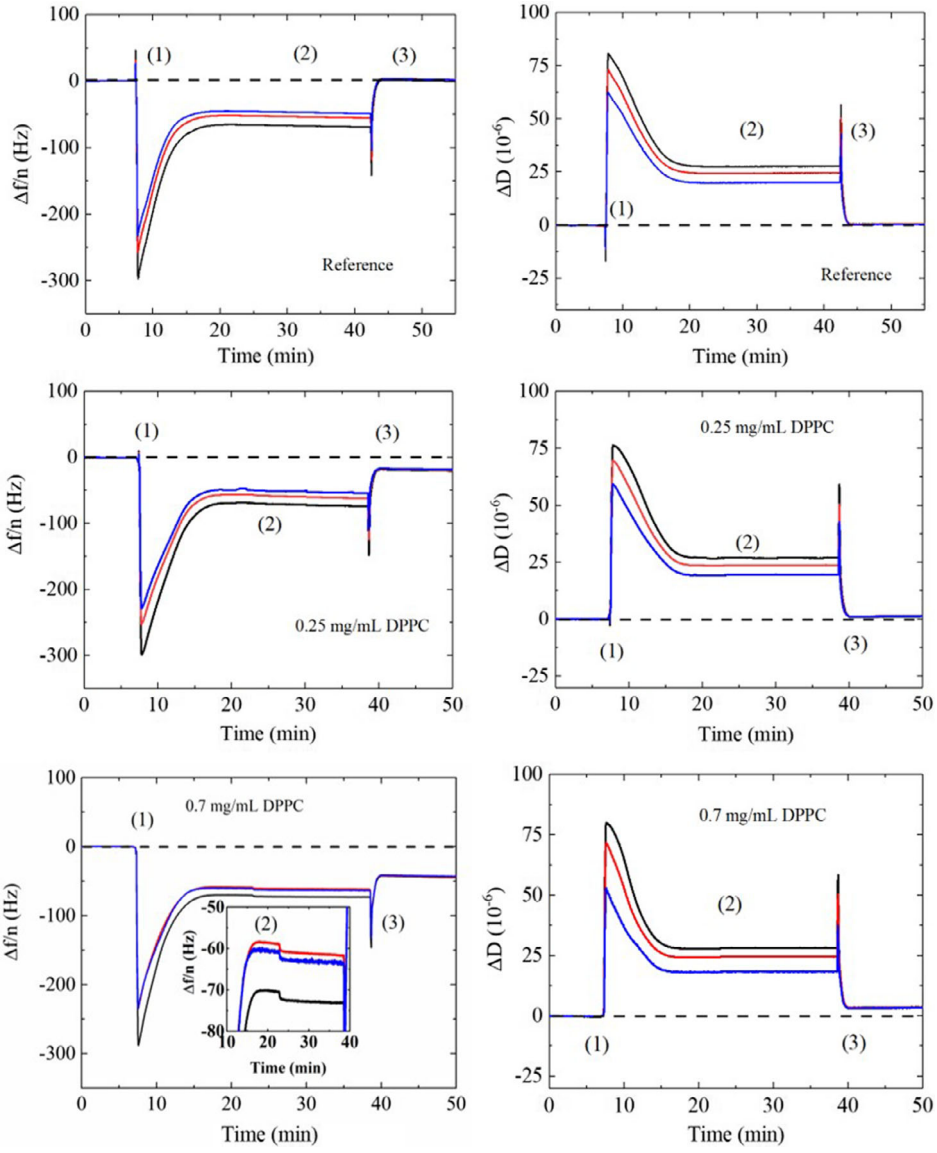

Figure 2. Time-dependent Δf_n and ΔD_n signals during the formation of SALB lipid layers by SALB. Upper panel: reference measurement, middle panel: 0.2 mg mL^{-1} DPPC lipid concentration, lower panel: 0.7 mg mL^{-1} DPPC lipid concentration. Solid lines: black 5th overtone, blue: 7th overtone, red: 9th overtone. Inset: small frequency shift due to monolayer and micelle adsorption at the solid/liquid interface.

Table 1. Plateau values after completion of the solvent exchange process monitored by QCM-D.

	Δf_7 [Hz]	$\Delta D_7 \times 10^{-6}$
Reference	<1	<0.5
0.2 mg mL^{-1} DPPC	-19 ± 1	1.3 ± 0.4
0.7 mg mL^{-1} DPPC	-43 ± 1	3.6 ± 0.3

Overall, the surface seems to be homogeneously covered by lipid layers. However, unlike for layers formed onto atomically flat surfaces such as mica, the underlying substrate roughness prevents distinguishing whether these are monolayers, bilayers, or multilayers by merely looking at the height measured. Figure 3c shows the surface after exposure to 0.7 mg mL^{-1} DPPC. The surface is more heterogeneous and covered with patches of 4–5 nm thickness and lateral sizes ranging from 12 to 25 nm, separated by areas that display the same morphology as the low concentration case. A few white spots on the surface with relatively high thickness can be seen and might be DPPC multilayers or nonruptured vesicles. The average roughness increases to $R_a = 2 \pm 2$ nm and clearly displays two populations, indicating that the surface is partially covered by SLB patches.

2.3. AFM Force Spectroscopy

Figure 4 shows representative force curves as a function of the tip–sample separation distance d during approach of an

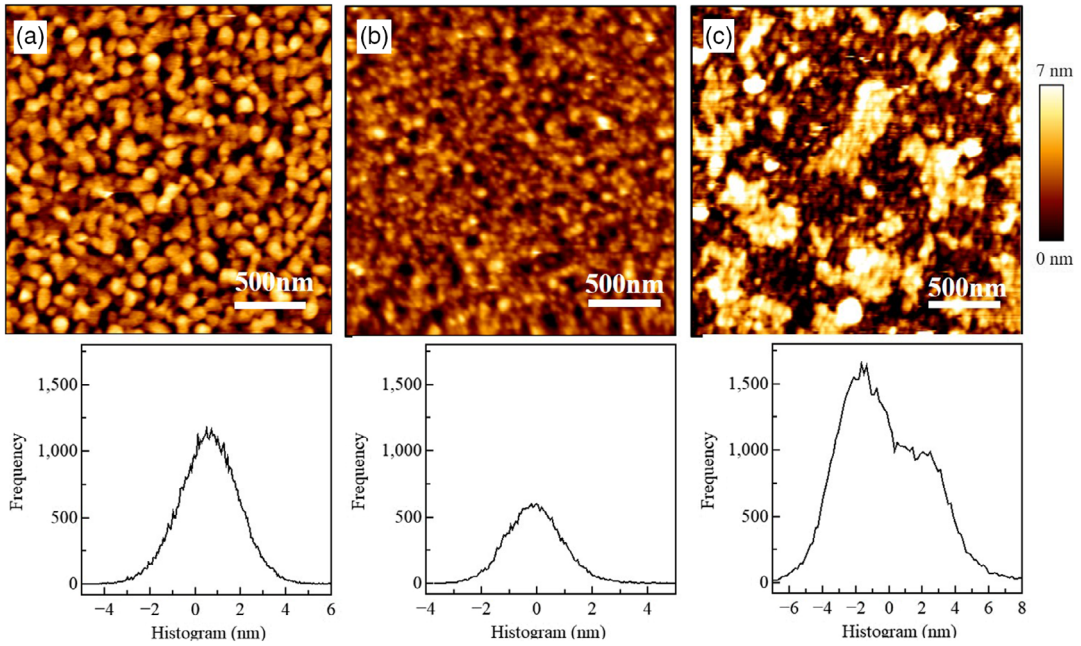

Figure 3. AFM height measured images with their corresponding surface roughness histogram of a) bare Au in HEPES buffer, b) 0.2 mg mL^{-1} DPPC, and c) 0.7 mg mL^{-1} DPPC with SALB method.

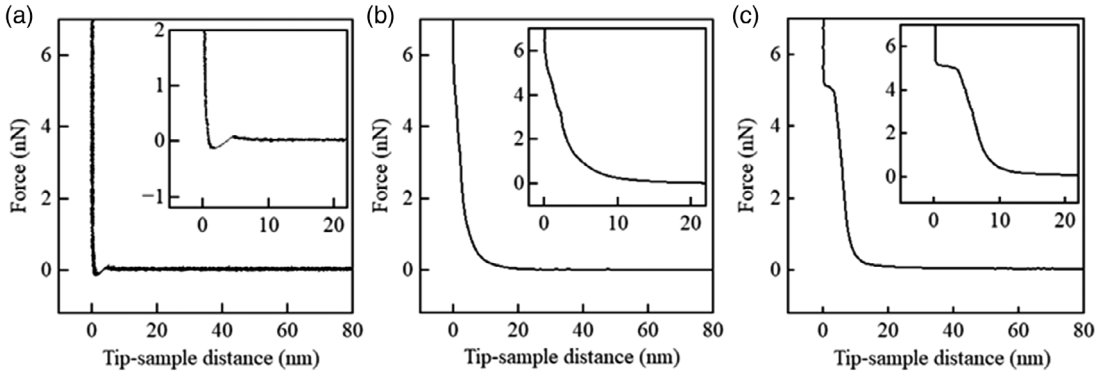

Figure 4. Extend *F–D* curves on a) bare Au sensor, b) DPPC monolayer, and c) DPPC bilayer.

Au-coated AFM tip to bare Au, and to Au-coated surfaces using SALB at low and high DPPC concentrations. The zero-separation distance $d = 0$ was defined as the point where the tip comes into an apparent hard contact with the surface. Upon approaching the Au-coated tip to the bare Au surface, no interaction is observed until $d = 0.5$ nm tip–surface vertical separation distance, when a weak attractive interaction is followed by a repulsive interaction at a very a small tip–surface separation ($d < 0.5$ nm). In the presence of films formed at low and high DPPC concentrations, the shape of the curves changes significantly. Films formed from low DPPC concentration in isopropanol display repulsive interactions between the tip and the lipid covered surface at separations <15 nm, while for films formed from high DPPC concentration, the curve starts deviating at separations ≈20 nm. Upon mechanical contact during approach, the supported lipid layer is elastically compressed (linear regime *F–D* curve) until the tip breaks through the layer, jumping in contact with the surface. The penetration of the AFM tip through the supported appears as a discontinuity in the approaching *F–D* curve (see Figure 4c). The vertical force at which this discontinuity takes place corresponds to the maximum force the bilayer is able to withstand before breaking and referred to as the breakthrough force (F_b) or yield threshold force.[28–30] F_b is regarded as a measurement of the lateral interactions within the lipid bilayer, at a fixed loading rate. The tip–sample distance at which penetration occurs gives an idea of the thickness of the lipid layer formed. For the particular example displayed in Figure 3, layers formed from low DPPC concentration SALB display a smooth discontinuity at ≈2.5 nm with a positive slope and $F_b \approx 3$ nN. Layers formed from high DPPC concentration SALB exhibit a clear jump-in feature at ≈4–5 nm with corresponding $F_b \approx 5.5$ nN.

In **Figure 5**a,c, representative figures of the two most abundant type of curves observed for layers formed at low DPPC concentration in isopropanol are included. Figure 5b,d shows the distribution of the measured breakthrough forces from at least 100 force curves as those shown in Figure 5a,b. In Figure 5a, repulsion starts around 10 nm tip–sample distance and a discontinuity in the force curve can be observed at around 2.5 nm. The breakthrough force F_b values were determined from the maximum of the Gaussian fits of the obtained histograms. The distance at which this discontinuity occurs points out at the presence of either a monolayer or tiny micelles, which represent about 85% of the total number of curves measured with an average F_b value of ≈2 nN. In Figure 5c, repulsion starts beyond 15 nm, followed by tip compression and jump-in step in the curve at separations of 5 nm (marked with black arrows), consistent with the presence of a single SLB.

Interestingly, the perforation of the single bilayer takes place in a two-step fashion, the sample–distance extent of each step being 3 and 2 nm. This effect is reminiscent of the leaflet decoupling observed in previous works at similar approaching tip speeds on freshly cleaved mica surfaces. Alessandrini et al. reported 1,2-dioleoyl-sn-glycero-3-phospho-rac-(1-glycerol) sodium salt force curves on mica at 27 °C, close to the bilayer main transition temperature and explained the decoupling observed as a consequence of fluctuations in the bilayer due to the proximity of the phase transition, which continuously shift the membrane from a coupled to an uncoupled state.[31] Adhyapak et al., in turn, observed that high cholesterol concentrations in DOPC bilayers induced asymmetry reflected in two jumps in the force curve at well-differentiated breakthrough forces. The authors invoked cholesterol reorganization within the leaflets to explain this two-step jump in observation. Cholesterol molecules are expelled from in between the leaflets and reorganize in the lower leaflets to attain equilibrium.[32] Earlier works on AFM force spectroscopy experiments reported double-step jump-ins using SiO_2 tips[33] or functionalized Au tips with mercapto-undecanol.[34] The former was ascribed to lipid structures deposited on the tip apex, both lipid material in the apex of the tip and that supported on the surface are compressed upon tip approach and displaced in two sequential steps. The latter displayed multiple breakthrough forces, which were ascribed to changes in the tip functionalization (lipid molecules picked by the functionalized tip) due to enhanced van der Waals attraction. In our case, layers are formed on polycrystalline Au, the DPPC lipid is in the gel phase at the temperature at which the experiments were performed, and the Au tip is not functionalized. It is worth noting that the occurrence of this two-step jump was observed in less than 15% of the force curves measured and the histograms do not display a clear maximum,

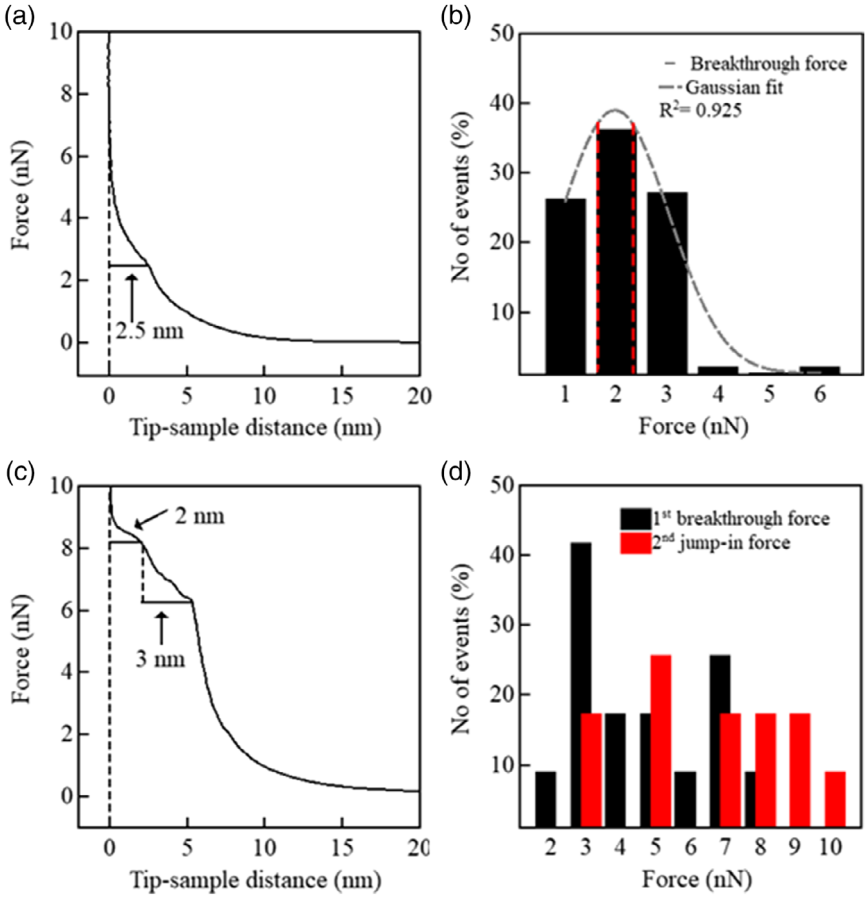

Figure 5. Example of AFM tip–sample distance versus force curves of 0.2 mg mL^{-1} DPPC in HEPES buffer by SALB on Au sensors: a) monolayer or small micelle and b) two-step jump bilayer with their corresponding histograms [panels (c) and (d)]. Dashed red vertical lines indicate 95% confidence intervals.

indicating that the occurrence of the two-step jump is rather aleatory. As will be shown for bilayers formed from high DPPC concentration in isopropanol, bilayers displaying a two-step jump were observed more frequently (around 40% of the force curves measured). Although one cannot rule out the possibility of the AFM tip picking up adsorbed lipid molecules and forming bilayer patches at the apex of the tip, we are more inclined to think that the two-step jump-in observed might be a reflection of bilayer leaflet decoupling, as a result of combined surface topography and the mechanism of SALB formation (starting from monolayer and inverted micelle adsorption).

An overview of the different types of force curves observed for layers formed at high DPPC concentration in isopropanol can be found in **Figure 6**. The force curves range from one-step supported bilayers (45%), two-step SLBs (34%), and double bilayers (19%). Very few curves (2%) show tip–sample repulsive interactions starting at longer distances, which could correspond to unruptured vesicles or micelles adsorbed on the surface, as previously mentioned in Figure 3c. Below each representative curve, a histogram summarizing the F_b values over 100 curves is included. The mean value of the Gaussian fitting is taken as the maximum of the Gaussian in each case. The average breakthrough force of the one-step bilayer is in the range of 5 ± 1 nN, as shown in Figure 6d, and the average tip–sample interaction distance between the tip and the surface is $\approx 4.5 \pm 1$ nm, a distance which corresponds to a slightly compressed SLB. When compared with DPPC lipid bilayers supported on mica or glass at room temperature, the average breakthrough force F_b for one-step bilayer formed by SALB is smaller. This difference can be partly ascribed to the differences in ionic strength and the absence of cations of the buffer used in this work compared with larger F_b values reported in the literature,[35] but mostly to the seldomly studied effect of the underlying surface roughness, which might weaken lateral interactions and thus yield smaller F_b values. Figure 6b shows an example of a curve where jump-ins taking place in two steps are observed. Figure 6d,e shows how the first jump-in breakthrough takes place at a force $F_{b1} \approx 5 \pm 1$ nN, while the second jump-in mean value $F_{b2} \approx 7 \pm 1$ nN. Figure 6c displays a *F–D* curve with a multiple jump-in event at different tip–sample interaction distances. The repulsive interaction starts at around 20 nm tip–sample separation, followed by compression of the layer and a first jump-in event at tip–sample separation of 10 nm, corresponding to the thickness of a solid-supported double lipid bilayer. A recent study of DPPC vesicles deposited on TiO_2 has exhibited clear signatures of vesicle rupture under repeated loading and unloading leading, first to very compressed double bilayer vesicles with similar nanomechanical signatures as the ones shown here and eventually to single SLBs.[36] In our case, subsequent loading did not change the shape of the curves, thus confirming that double supported bilayers were initially formed. Yet, nanomechanical signatures corresponding to adsorbed vesicles/micelles from the process were found in 2% of the curves. A representative force curve can be found in Figure S1, Supporting Information.

Representative retract curves as a function of the tip–sample separation distance for bare Au, and Au-coated surfaces using

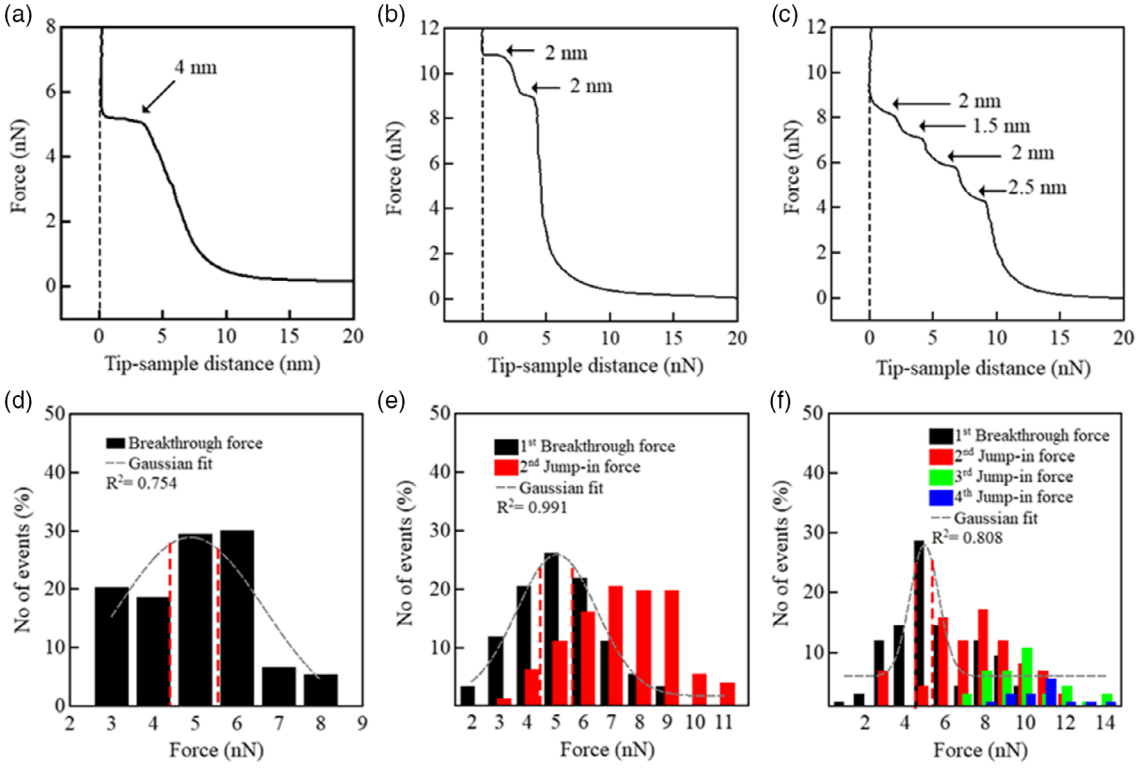

Figure 6. Example of AFM tip–sample distance versus force curves of 0.7 mg mL^{-1} DPPC in HEPES buffer by SALB on Au sensors: a) one-step jump bilayer, b) two-step jump bilayer, and c) double bilayer with their corresponding histograms [panels (d), (e), and (f)]. The numbers and arrows indicate the size (tip–sample distance) of jump-in events. Dashed red vertical lines indicate 95% confidence intervals.

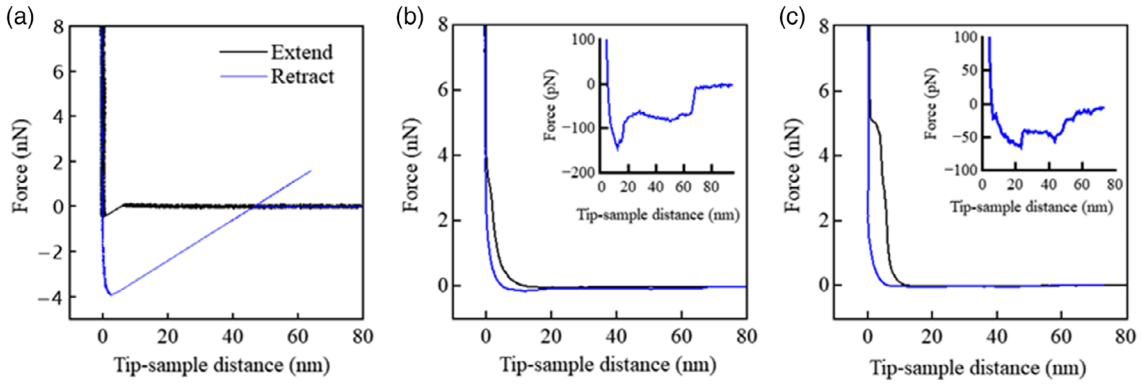

Figure 7. Typical AFM tip–sample interaction curves on a) bare Au, b) with low, and c) with high concentration of DPPC in isopropanol. Inset of (b) and (c): zoom-in plot to see the tube features.

SALB at low and high DPPC concentrations are shown in **Figure 7**. Upon retraction, a very large adhesion force (up to 4 nN in absolute value) is observed on bare Au due to a strong interaction of the surface with the Au-coated tip, in agreement with a large Hamaker constant of Au–Au interactions in aqueous medium.[37] When supported lipid layers are present on the Au surface, the adhesive force is significantly reduced as consequence of the weaker interactions between the Au-coated tip and supported lipid molecules. Unlike for bare Au, a clear hysteresis between approach and retract curves at short tip–separation distances is observed on lipid-coated surfaces formed both at low and high DPPC concentration in isopropanol. Hysteresis is typically ascribed to energy dissipation during healing of the adsorbed bilayer after having been perforated and is related to the viscoelastic character of the formed layers.[38] In some cases, upon subsequent tip retraction, a small constant negative force was observed at distances of tens of nm until the tip return to the equilibrium (zero-force) position. This process illustrates the pulling of tube-like structures from the supported lipid layers that remain connected upon retraction of the tip. The tube grows at constant force, the tube growing force F_{tube} until it breaks at a certain distance, tube growing distance d_{tube}, where a step can be observed, and the cantilever returns to the equilibrium position.[39,40] In this work, tube pulling has been mainly observed on supported lipid layers formed at high DPPC concentration in isopropanol (≈30% of the analyzed curves), while layers formed at low DPPC concentration were observed occasionally (for less of <10% of the analyzed curves). Histograms from which mean values of $F_{\text{tube}} \approx 43$ pN and $L_{\text{tube}} \approx 47$ nm for SLBs formed at high DPPC concentration can be found in Figure S2, Supporting Information.

3. Conclusion

This work has reported a combined experimental study to assess the effect of lipid concentration in organic solvent when forming supported membranes by SALB on a polycrystalline Au surface. DPPC was used as model zwitterionic phospholipid at two limiting concentration values within the optimal reported conditions from previous literature reports to achieve the formation of homogeneous SLBs. Combining QCM-D with AFM topographical and nanomechanical measurements provided a more complete qualitative picture of the different layers formed.

QCM-D plateau values upon fulfillment of the SALB process depart slightly from those characterizing the formation of a homogeneous SLB, suggesting the formation of inhomogeneous layers. When imaged by AFM, the layers formed at low and high concentration differ significantly; the former yield more homogeneous, smoother topographies, while the latter display heterogeneous surfaces covered with nanometer-scaled patches bearing thickness commensurate with single and double SLBs. Nanomechanical measurements shed more light into the type of layers present on the Au surface. The majority of force curves recorded onto layers formed at low DPPC concentration point toward the predominance of monolayer-thick structures bearing weak intermolecular forces, whereas very few bilayers-like structures could be detected likely to a shortage of lipid molecules at low concentration. In turn, force curves recorded onto layers formed at high DPPC concentration display a more diverse with a large percentage of bilayer-thick structures with a smaller breakthrough force as compared with mica or glass counterparts. Upon tip compression and penetration of the layer, half of the curves displayed two-step jump-in events, which might be account for bilayer leaflet decoupling. Despite the surface coverage is not fully controllable using SALB, the formed lipid assemblies at different concentrations constitute a promising testing ground for decoupling the effect of surface roughness on supported lipid organization for metallic surfaces. Further efforts will be oriented toward the use of Au surfaces of increasing topographical complexity, ranging from grain boundary-, atomically flat single crystals, atomically flat polycrystalline (template stripped) Au surfaces to Au surfaces with well-controlled nanotopography.

4. Experimental Section

Materials: DPPC was purchased from Avanti Polar Lipids (Alabaster, AL). Hydrogen peroxide (30%) and sodium dodecyl sulfate (SDS) were purchased from Merck, Belgium. Isopropanol (assay 99.7%) (IPA), absolute ethanol (assay 99.85%), and ammonia (25%) were purchased from VWR Prolab Chemicals, Belgium. HEPES buffer (pH 7.4) consisted of 10 mM HEPES (99%) and 150 mM NaCl, both from Sigma-Aldrich (≥99.5%). Ultrapure water with conductivity of 18.2 MΩ cm (at 25 °C)

was obtained from a Simplicity device (Millipore, France) and was used to prepare the aqueous solutions. Au-coated quartz sensors were cleaned with a 5:1:1 mixture of ultrapure water:hydrogen peroxide (30%):ammonia (25%) at 70 °C for each measurement. The used QCM-D sensors and their accessories were cleaned with a solution containing 2% sodium dodecyl sulfate in ultrapure water. DPPC was dissolved in IPA to get the concentrations of 0.2 and 0.7 mg mL^{-1}, respectively, for the SALB experiments. The lipid masses were determined gravimetrically using an analytical balance (AG245, Metter-Toledo, Switzerland) with a weighing precision of ±0.1 mg.

Contact Angle Measurements: Water contact angle (WCA) of the Au-coated sensors was measured by the sessile drop method using an Attension ThetaLite instrument from Biolin Scientific (Sweden) to confirm the hydrophilic character of the surfaces. A water droplet of 3 µL was dropped on the Au surface with a recording speed of 20 frames s^{-1} for 10 s. The contact angle was measured in at least three spots in each sensor. The average water contact angle for UV–ozone-treated Au sensors is ≈11 ± 2°.

QCM-D Monitoring: QCM-D measurements were conducted by using Au-coated AT-cut quartz crystals (Qsense, Biolin Scientific, Sweden) on a Q-sense E4 instrument (LOT-Quantum Design, Belgium). These polycrystalline Au crystal sensors bear a diameter of 14 mm and a thickness of 0.3 mm. QCM-D measures the changes in resonance frequency Δf and energy dissipation ΔD of an oscillating quartz sensor when mass is adsorbed on it. The changes in resonance frequency Δf are obtained form (hydrated) mass changes, and ΔD from $D = E_{lost}/2\pi E_{stored}$, where E_{lost} is the energy dissipated during one oscillation and E_{stored} is the energy stored. The dissipation is related to changes in the viscoelastic properties of the adsorbed film. All QCM-D measurements were conducted recording both the frequency and the dissipation shifts for five overtones (3rd, 5th, 7th, 9th, 11th). The sensors were cleaned before each measurement by the protocol explained in the previous section. UV–ozone treatment for 20 min activated the Au surfaces before placing the sensors in the QCM-D flow cell. SALB measurements were performed at 25 °C. The actual procedure of SALB measurements is explained in detail in Section 2.1.

AFM: AFM imaging and force spectroscopy measurements were performed using a JPK NanoWizard 3 (JPK Instruments AG, Berlin, Germany). All the measurements were done in liquid mode AFM by using a home-made AFM flow cell. Contact mode imaging and force spectroscopy were conducted using a gold-coated tip (SHOCONGG-20, AppNano, USA) with quoted cantilever length of ≈225 µm, resonance frequency ≈21 kHz, and nominal spring constant ≈0.1 N m^{-1}. The probe was cleaned by dipping in 95% H_2SO_4, ultrapure water, and absolute ethanol, respectively, for 1 min each and dried with a gentle N_2 stream. The freshly cleaned tip was calibrated on a clean Au surface both in air and in Milli-Q water. Probe sensitivities and spring constant values were obtained by tip–sample *F–D* curve profiles during the tip calibration. Surface topography was scanned on different image sizes using a pixel ratio of either 256 × 256 or 512 × 512 with the tip line rate of 1 Hz, and *F–D* curves were recorded by using preset forces of 5, 10, and 15 nN with a tip speed of 2 µm s^{-1}. AFM experiments were conducted at 20 °C.

Supporting Information

Supporting Information is available from the Wiley Online Library or from the author.

Acknowledgements

P.L.P. acknowledges funding of the projects n. 20061 "SADI" by the program Action Recherche Concertée, Université Libre de Bruxelles (ULB) and SurfTBiomem project n. F.4525.20 by the "Fonds de la Recherche Scientifique" (FNRS). S.N. and F.U.R. acknowledge financial support from FWO Odysseus program under G0D0115N project.

Conflict of Interest

The authors declare no conflict of interest.

Keywords

atomic force microscopy, biointerfaces, quartz crystal microbalance with dissipation, solvent exchange, supported lipid membranes

Received: October 24, 2020
Revised: December 13, 2020
Published online:

[1] E. T. Castellana, P. S. Cremer, *Surf. Sci. Rep.* **2006**, *61*, 429.
[2] R. Glazier, K. Salaita, *Biochim. Biophys. Acta* **2017**, *1859*, 1465.
[3] R. P. Richter, R. Bérat, A. R. Brisson, *Langmuir* **2006**, *22*, 3497.
[4] R. Tero, *Materials* **2012**, *5*, 2658.
[5] I. Czolkos, A. Jesorka, O. Orwar, *Soft Matter* **2011**, *7*, 4562.
[6] G. J. Hardy, R. Nayak, S. Zauscher, *Curr. Opin. Colloid Interface Sci.* **2013**, *18*, 448.
[7] U. Mennicke, T. Salditt, *Langmuir* **2002**, *18*, 8172.
[8] H. C. González, U. G. Volkmann, M. J. Retamal, M. Cisternas, M. A. Sarabia, K. A. López, *J. Chem. Phys.* **2012**, *136*, 134709.
[9] R. Lipowsky, U. Seifert, *Mol. Cryst. Liq. Cryst.* **1991**, *202*, 17.
[10] R. Richter, A. Mukhopadhyay, A. Brisson, *Biophys. J.* **2003**, *85*, 3035.
[11] S. K. Pramanik, S. Seneca, A. Ethirajan, S. Neupane, F. U. Renner, P. Losada-Pérez, *Biointerphases* **2016**, *11*, 019006.
[12] T. K. Lind, M. Cárdenas, *Biointerphases* **2016**, *11*, 020801.
[13] M. Li, M. Chen, E. Sheepwash, C. L. Brousseau, H. Li, B. Pettinger, H. Gruler, J. Lipowsky, *Langmuir* **2008**, *24*, 10313.
[14] C. A. R. Chapman, H. Chen, M. Stamou, J. Biener, M. M. Biener, P. J. Lein, E. Seker, *ACS Appl. Mater. Interfaces* **2015**, *7*, 7093.
[15] S. R. Tabaei, J. A. Jackman, S.-O. Kim, V. P. Zhdanov, N. J. Cho, *Langmuir* **2015**, *31*, 3125.
[16] S. R. Tabaei, J. H. Choi, G. H. Zan, V. P. Zhdanov, N. J. Cho, *Langmuir* **2014**, *30*, 10363.
[17] S. R. Tabaei, J. A. Jackman, S.-O. Kim, B. Liedberg, W. Knoll, A. N. Parikh, N. J. Cho, *Langmuir* **2014**, *30*, 13345.
[18] S. R. Tabaei, S. Vafaei, N. Cho, *Phys. Chem. Chem. Phys.* **2015**, *17*, 11546.
[19] J. J. J. Gillissen, S. R. Tabaei, N. J. Cho, *Phys. Chem. Chem. Phys.* **2016**, *18*, 24157.
[20] M. C. Kim, J. J. J. Gillissen, S. R. Tabaei, V. P. Zhdanov, N. J. Cho, *Phys. Chem. Chem. Phys.* **2015**, *17*, 31145.
[21] A. R. Ferhan, B. K. Yoon, S. Park, T. N. Sut, H. Chin, J. H. Park, J. A. Jackman, N. J. Cho, *Nat. Protocols* **2019**, *14*, 2091.
[22] H. Chin, J. J. J. Gillissen, E. Miyako, N. J. Cho, *Rev. Sci. Instrum.* **2019**, *90*, 033707.
[23] K. Betlem, G. Cordoyiannis, P. Losada-Pérez, *Phys. Status Solidi A* **2019**, *217*, 1900837.
[24] P. Losada-Pérez, O. Polat, A. N. Parikh, E. Seker, F. U. Renner, *Biointerphases* **2018**, *13*, 011002.
[25] A. O. Hohner, M. P. C. Daid, J. O. Rädler, *Biointerphases* **2010**, *5*, 1.
[26] T. Maekawa, H. Chin, T. Nyu, T. N. Sut, A. R. Ferhan, T. Hayashi, N. J. Cho, *Phys. Chem. Chem. Phys.* **2019**, *21*, 16686.
[27] D. Lichtenberg, C. Schmidt, *Lipids* **1981**, *16*, 555.
[28] Y. F. Dufrêne, W. R. Barger, J. B. D. Green, G. U. Lee, *Langmuir* **1997**, *13*, 4779.
[29] S. García-Manyés, L. Redondo-Morata, G. Oncins, F. Sanz, *J. Am. Chem. Soc.* **2010**, *132*, 12874.

[30] L. Redondo-Morata, M. I. Giannotti, F. Sanz, *Langmuir* **2012**, *28*, 12851.
[31] A. Alessandrini, H. M. Seeger, T. Caramaschi, P. Facci, *Biophys. J.* **2012**, *103*, 38.
[32] P. R. Adhyapak, S. V. Panchal, A. V. R. Murthy, *Biochim. Biophys. Acta Biomem.* **2018**, *1860*, 953.
[33] R. P. Richter, A. Brisson, *Langmuir* **2003**, *19*, 1632.
[34] I. Pera, R. Stark, M. Kappl, H. J. Butt, F. Benfenati, *Biophys. J.* **2004**, *87*, 2446.
[35] L. Redondo-Morata, G. Oncins, F. Sanz, *Biophys. J.* **2012**, *102*, 66.
[36] Y. Duan, Y. Liu, J. Li, H. Wang, S. Wen, *Polymers* **2018**, *10*, 383.
[37] F. L. Leite, C. C. Bueno, A. L. Da Róz, E. C. Ziemath, O. N. Oliveira Jr., *Int. J. Mol. Sci.* **2012**, *13*, 12773.
[38] L. M. Grant, F. Tiberg, *Biophys. J.* **2002**, *82*, 1373.
[39] A. Roux, *Soft Matter* **2013**, *9*, 6726.
[40] B. Gumí-Audenis, L. Costa, L. Ferrer-Tasies, I. Ratera, N. Ventosa, F. Sanz, M. I. Giannotti, *Nanoscale* **2018**, *10*, 14763.